LA-UR-17-29286
Approved for public release; distribution is unlimited.

Title: An anisotropic elastoplasticity model implemented in FLAG

Author(s): Buechler, Miles Allen
Canfield, Thomas R.

Intended for: Report

Issued: 2017-10-12

An anisotropic elastoplasticity model implemented in FLAG

Miles A. Buechler and Tom Canfield

Los Alamos National Laboratory

Los Alamos, NM 87545

buechler@lanl.gov

Executive Summary

Many metals, including Tantalum and Zirconium, exhibit anisotropic elastoplastic behavior at the single crystal level, and if components are manufactured from these metals through forming processes the polycrystal (component) may also exhibit anisotropic elastoplastic behavior. This is because the forming can induce a preferential orientation of the crystals in the polycrystal. One example is a rolled plate of Uranium where the stiff/strong orientation of the crystal (c-axis) tends to align itself perpendicular to the rolling direction. If loads are applied to this plate in different orientations the stiffness as well as the flow strength of the material will be greater in the through thickness direction than in other directions. To better accommodate simulations of such materials, an anisotropic elastoplasticity model has been implemented in FLAG. The model includes an anisotropic elastic stress model as well as an anisotropic plasticity model. The model could represent single crystals of any symmetry, though it should not be confused with a high-fidelity crystal plasticity model with multiple slip planes and evolutions. The model is most appropriate for homogenized polycrystalline materials. Elastic rotation of the material due to deformation is captured, so the anisotropic models are appropriate for arbitrary large rotations, but currently they do not account for significant change in material texture beyond the elastic rotation of the entire polycrystal.

1 Motivation

Many components are manufactured through some forming process. One such process is the rolling of flat plates. The material undergoes very large plastic deformation during the rolling process, which can cause non-uniform texture to evolve. This texture evolution causes anisotropic material behavior, which can have significant impact on the response of components to loads. An example is shown in Figure 1. A Taylor rod was simulated using anisotropic properties for Tantalum [3]. The asymmetry of the deformation is significant as can be seen in Figure 1b.

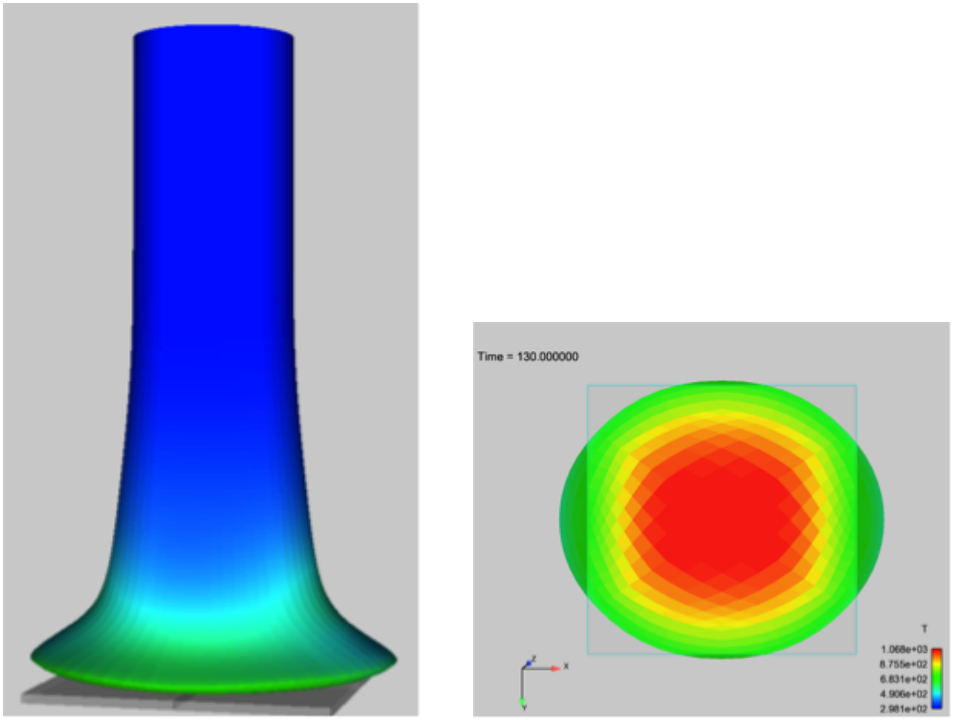

(a) Deformed Taylor Rod

(b) Foot print

Figure 1: Simulation of a Taylor Rod experiment with an anisotropic material. An isotropic Rod would deform to have a circular footprint. The square helps to demonstrate the level of anisotropic flow.

A schematic of a rolled plate and texture measurements from partially annealed depleted Uranium (DU) is shown in Figure 2. The pole figures are a projection of a hemisphere of measurements. The center of those measurements is normal to the rolled plate. The three plots are labeled 001, 010, and 100, but they can also

be thought of as the c, b, and a axis of a Uranium crystal, respectively. The scale contours are related to the probability that a crystal's axis is pointed in the direction on the hemisphere (which is projected to a plane). Take the 001 plot as an example. The red color centered on the origin indicates that there is a high probability of finding crystals with the c-axis pointed normal to the plate. The quantity being plotted is multiples of random distribution (MRD), which means that a crystal c axis is about 5 times more likely to point normal to the plate than a uniformly random distribution of crystals. Also note that the distribution is elliptical with the minor axis in the final rolling direction (RD). There are more a-axis and b-axis pointed in the plane of the plate indicated by the edge of the projected sphere. Finally, there is a higher probability of finding b-axis pointed in the final rolling direction than in the final transverse direction (TD).

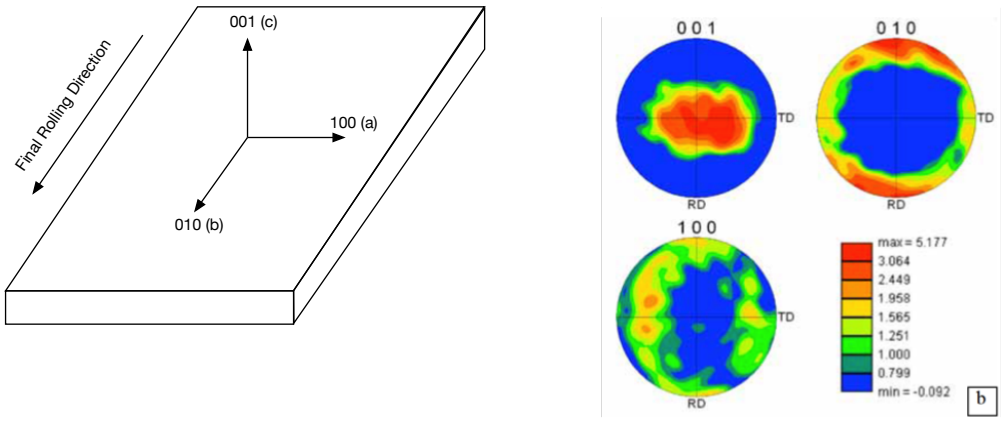

(a) Rolled Plate

(b) Texture

Figure 2: Schematic of rolled plate and material texture measurements courtesy of Rodney McCabe [1]

2 Anisotropic elastoplastic model

Several new material nodes have been added to FLAG to support modeling of anisotropic materials. These nodes can capture anisotropic elastic and plastic behavior.

2.1 Elastic model

The deviatoric elastic response is calculated using a rate form. Storage and computational efficiency are achieved using b-basis transforms [3], but the model can be easily understood as

$$\boldsymbol{\sigma}_{n+1} = \boldsymbol{\sigma}_n + \mathbb{C} : \boldsymbol{D}, \tag{1}$$

where $\boldsymbol{\sigma}$ is the stress, $\mathbb{C}$ is the stiffness tensor, and $\boldsymbol{D}$ is the symmetric part of the velocity gradient. Many models in FLAG can incorporate a Juaman rate that updates the old stress to account for rotations. In the anisotropic model the stiffness tensor is attached to the material, so we incorporate Algorithm 1 to rotate the old stress and the velocity gradient back to the material frame. The stress is updated in the material frame and the new stress is rotated forward to the laboratory frame.

Algorithm 1 Stress Update

Input: `VARS` : $\boldsymbol{\sigma}_n$, $\boldsymbol{D}$, $\boldsymbol{R}_n$, $\boldsymbol{L}$ `PARAMS` : $\mathbb{C}$

Output: $\boldsymbol{\sigma}_{n+1}$

1: $\hat{\boldsymbol{\sigma}}_n = \boldsymbol{R}_n^T \boldsymbol{\sigma} \boldsymbol{R}_n, \quad \hat{\boldsymbol{D}} = \boldsymbol{R}_n^T \boldsymbol{D} \boldsymbol{R}_n$

2: $\hat{\boldsymbol{\sigma}}_{n+1} = \hat{\boldsymbol{\sigma}}_n + \mathbb{C} : \hat{\boldsymbol{D}}$

3: **update** $\boldsymbol{R}$ using Taylor Flanagan Algorithm using $\boldsymbol{L}$

4: $\boldsymbol{\sigma}_{n+1} = \boldsymbol{R}_{n+1} \hat{\boldsymbol{\sigma}}_{n+1} \boldsymbol{R}_{n+1}^T$

This algorithm happily handles large rotations of the material. It should be noted that it does not at this time capture significant change in texture, which would result in a changing stiffness tensor and potentially changes in the plasticity. The base node for anisotropic elasticity is found at:

/global/mesh/mat/solid/model/decoupled/estress/aniso.

All the crystal symmetry classes are supported and can be found under the aniso node.

2.2 Plastic flow model

The above development assumes all the deformation is elastic. To incorporate the anisotropic plastic behavior we partition the deformation into elastic and plastic parts as

$$\boldsymbol{D} = \boldsymbol{D}^e + \boldsymbol{D}^p, \tag{2}$$

where $\boldsymbol{D}^p$ is the elastic part, and we would replace the total deformation rate in the elastic model above with the elastic part:

$$\boldsymbol{D}^e = \boldsymbol{D} - \boldsymbol{D}^p. \tag{3}$$

This section describes the process for calculating the plastic part of the deformation rate.

We start by defining an effective stress ($\bar{\sigma}$) that describes the anisotropic behavior. The effective stress used here is [2]

$$\bar{\sigma} = \sqrt{\frac{3}{2} S \cdot \boldsymbol{\alpha} \cdot S}, \tag{4}$$

where $\boldsymbol{S}$ is the deviatoric stress, and $\boldsymbol{\alpha}$ is a 4th order tensor that describes the anisotropy of plastic flow. Note that the plasticity community has commonly used a scale factor of $\frac{3}{2}$ as well as $\frac{1}{2}$. Here we use $\frac{3}{2}$, so the components of our $\boldsymbol{\alpha}$ are $\frac{1}{3}$ that of some implementations.

The plastic deformation rate is

$$\dot{\boldsymbol{D}}^p = \dot{\lambda}\boldsymbol{\eta} = 3\dot{\lambda}\boldsymbol{S}\alpha, \tag{5}$$

where $\dot{\lambda}$ is the plastic multiplication factor, which is found through an iterative process that determines the plastic multiplier that puts the effective stress back on the yield surface like any radial return algorithm. Note that, as in the elasticity model, the stress must be rotated into the material frame. Thus, the plastic deformation rate is already in the material rate. The anisotropic plastic flow node can be found at /global/mesh/mat/solid/model/decoupled/pflow/aniso_af. Under the aniso_af node sits two options for defining the $\boldsymbol{\alpha}$ tensor. They are **general** and **hill48**. In the general node you must provide 21 parameters for the $\boldsymbol{\alpha}$ tensor. The hill model requires 6 parameters.

NOTE: It is appropriate to note that while we define the effective stress using the $\frac{3}{2}$ scale factor we expect the parameters of $\boldsymbol{\alpha}$ in the form appropriate to the $\frac{1}{2}$ scale factor. On initialization, FLAG divides the inputs for $\boldsymbol{\alpha}$ by 3.

2.3 Initial Orientation

It is likely that the material orientation in a component may not line up with the global coordinate system. If this is the case an orientation can be initialized using Rodrigues vectors and angles to represent the initial rotation $\boldsymbol{R}_0$. There is an excellent writeup of Rodrigues vectors at Wikipedia (Search: Rodrigues' Rotation Formula), but we will reproduce the relevant parts here.

You can define a rotation tensor using a vector and an angle of rotation about the vector. The relationship is

$$\boldsymbol{R} = \exp\left(\theta \boldsymbol{K}\right), \tag{6}$$

where $\boldsymbol{K}$ is a skew symmetric tensor of the form

$$\boldsymbol{K} = \begin{bmatrix} 0 & -n_z & n_y \\ n_z & 0 & n_x \\ -n_y & -n_x & 0 \end{bmatrix}, \tag{7}$$

where n_x, n_y, and n_z are the components of the vector. Ostensibly, we have an initial rotation tensor, and we want to find the vector and angle. To do that, first invert Equation 6

$$\theta \boldsymbol{K} = \log\left(\boldsymbol{R}\right), \tag{8}$$

which is a matrix. Then assemble the vector $\langle n_x, n_y, n_z \rangle$ and normalize it to length 1. θ is the normalizing factor.

Of course, the exp and log functions used above are matrix versions of these functions, but most mathematical packages include a suitable form.

3 Model implementation specifics: b-basis

Because the plasticity model operates on a deviatoric stress tensor, which has a redundant component[1], we employ a b-basis transform to reduce the number of components from six to five. The transformation, described by Paul Maudlin [3], is partially reproduced here for completeness. The deviatoric stress is decomposed using a set of orthonormal basis tensors using the summation

$$\boldsymbol{S} = \sum_{k=1}^{5} \tau_k \boldsymbol{B}_k, \tag{9}$$

The B tensors have the property,

$$\boldsymbol{B}_i : \boldsymbol{B}_j = \delta_{ij}, \tag{10}$$

so you can also write

$$\tau_k = \boldsymbol{S} : \boldsymbol{B}_k, \tag{11}$$

where τ_k are the b-basis stress components. The plastic shape tensor, α, can also be decomposed using b-basis as

$$\alpha = \sum_{i=1}^{5} \sum_{j=1}^{5} \alpha_{ij}^{b} \boldsymbol{B}_i \otimes \boldsymbol{B}_j. \tag{12}$$

Using the $\boldsymbol{B}$ tensors, defined in Maudlin's paper [3], we can define a transform tensor $\boldsymbol{T}$ to be

$$\boldsymbol{T} = \begin{bmatrix} -\sqrt{2}/2 & \sqrt{2}/2 & 0 & 0 & 0 & 0 \\ -\sqrt{6}/6 & -\sqrt{6}/6 & \sqrt{6}/3 & 0 & 0 & 0 \\ 0 & 0 & 0 & 0 & 0 & \sqrt{2} \\ 0 & 0 & 0 & 0 & \sqrt{2} & 0 \\ 0 & 0 & 0 & \sqrt{2} & 0 & 0 \\ -1/3 & -1/3 & -1/3 & 0 & 0 & 0 \end{bmatrix}. \tag{13}$$

Note the placement of the $\sqrt{2}$ in the shear terms of the transform tensor. This is to swap between the FLAG ordering of tensor components and the crystal plasticity ordering. We can now write

$$\tau = \boldsymbol{T} \cdot \sigma, \tag{14}$$

[1]The trace of the deviatoric stress tensor is 0. Therefore, given two diagonal components, the third is known.

where τ_1-τ_5 are the b-basis stresses given by Equation 15

$$\begin{pmatrix} \tau_1 \\ \tau_2 \\ \tau_3 \\ \tau_4 \\ \tau_5 \end{pmatrix} = \begin{pmatrix} (S_{22} - S_{11})/\sqrt{2} \\ \sqrt{3/2} S_{33} \\ \sqrt{2} S_{23} \\ \sqrt{2} S_{31} \\ \sqrt{2} S_{12} \end{pmatrix}, \tag{15}$$

and τ_6 is the pressure. The b-basis shape tensor is

$$\boldsymbol{\alpha}^b = \boldsymbol{T} \cdot \boldsymbol{\alpha} \cdot \boldsymbol{T}^{-1}, \tag{16}$$

so for a 6 parameter Hill48 model

$$\boldsymbol{\alpha}^b = \begin{bmatrix} f & h & 0 & 0 & 0 \\ h & g & 0 & 0 & 0 \\ 0 & 0 & l & 0 & 0 \\ 0 & 0 & 0 & m & 0 \\ 0 & 0 & 0 & 0 & n \end{bmatrix}, \tag{17}$$

where the b-basis parameters f thru n are related to the more standard Hill48 parameters F thru N by

$$\begin{pmatrix} f \\ g \\ h \\ l \\ m \\ n \end{pmatrix} = \begin{pmatrix} \frac{1}{2}(F + G + 4H) \\ \frac{3}{2}(F + G) \\ \frac{\sqrt{3}}{2}(G - F) \\ L \\ M \\ N \end{pmatrix}. \tag{18}$$

4 Process of fitting the plastic flow shape tensor (α) to experimental plasticity data

Here we will try to describe the process of fitting the Hill48 model to experimental data. In an ideal world we would start with a well characterized microstructure (pole figures), so that we can identify planes of symmetry. We would then perform six (plus repeats) experiments on the material. These experiments would include three uniaxial experiments (in three orthogonal directions) and three in plane shear experiments (the three planes are defined by the three orthogonal vectors). Applying Equation 4, the effective stress at yield for each of those experiments is

$$\begin{aligned}
\bar{\sigma}_1 &= \sigma_{1y}\sqrt{\tfrac{3}{2}\left(G+H\right)} \\
\bar{\sigma}_2 &= \sigma_{2y}\sqrt{\tfrac{3}{2}\left(F+H\right)} \\
\bar{\sigma}_3 &= \sigma_{3y}\sqrt{\tfrac{3}{2}\left(F+G\right)} \\
\bar{\sigma}_4 &= \sigma_{4y}\sqrt{3L} \\
\bar{\sigma}_5 &= \sigma_{5y}\sqrt{3M} \\
\bar{\sigma}_6 &= \sigma_{6y}\sqrt{3N}
\end{aligned} \quad , \tag{19}$$

where the over-bars indicate the effective stress at yield, and the subscript #y indicates the applied stress at yield in the #direction. In this framework we must use a single flow stress model, so we impose: $\bar{\sigma}_1 = \bar{\sigma}_2 = \bar{\sigma}_3 = \bar{\sigma}_4 = \bar{\sigma}_5 = \bar{\sigma}_6 = \bar{\sigma}$. It might be convenient to set $\bar{\sigma}$ to one of the measured yield stresses, or do as is done in Section 6. Next, we define the yield stress ratios $R_i = \frac{\bar{\sigma}}{\sigma_{iy}}$ and solve the linear equations resulting in

$$\begin{aligned}
F &= -\tfrac{R_1^2}{3} + \tfrac{R_2^2}{3} + \tfrac{R_3^2}{3} \\
G &= \tfrac{R_1^2}{3} - \tfrac{R_2^2}{3} + \tfrac{R_3^2}{3} \\
H &= \tfrac{R_1^2}{3} + \tfrac{R_2^2}{3} - \tfrac{R_3^2}{3} \\
L &= \tfrac{1}{3}R_4^2 \\
M &= \tfrac{1}{3}R_5^2 \\
N &= \tfrac{1}{3}R_6^2
\end{aligned} \quad . \tag{20}$$

In the current implementation the $\boldsymbol{\alpha}$ tensor does not evolve with plastic strain or rate, so these should be determined from reasonably representative rates. If the material behavior is well represented with a constant tensor, quasi-static experiments would work as well as any.

5 Additional steps necessary to fit a flow stress model to experimental data

The previous section discussed fitting of the parameters in the $\boldsymbol{\alpha}$ tensor to experimental data. That step requires only stress at the onset of yield. If a hardening or rate dependent flow stress model is to be used additional steps must be taken to fit its parameters to experimental data. An example set of data, provided by Shuh-Rong Chen [1], is shown in Figure 3. The figure shows lot to lot variability, but it is clear that there is an orientation/texture effect on the stress-strain behavior. The strain axis in the figure is the measured strain in the direction of loading. Unlike a Mises plasticity model, the equivalent plastic strain that is appropriate for calculating hardening behavior is not simply the measured strain in the direction of loading. In fact, the ratio of equivalent plastic strain to the measured strain is different in each direction and dependent on the α tensor.

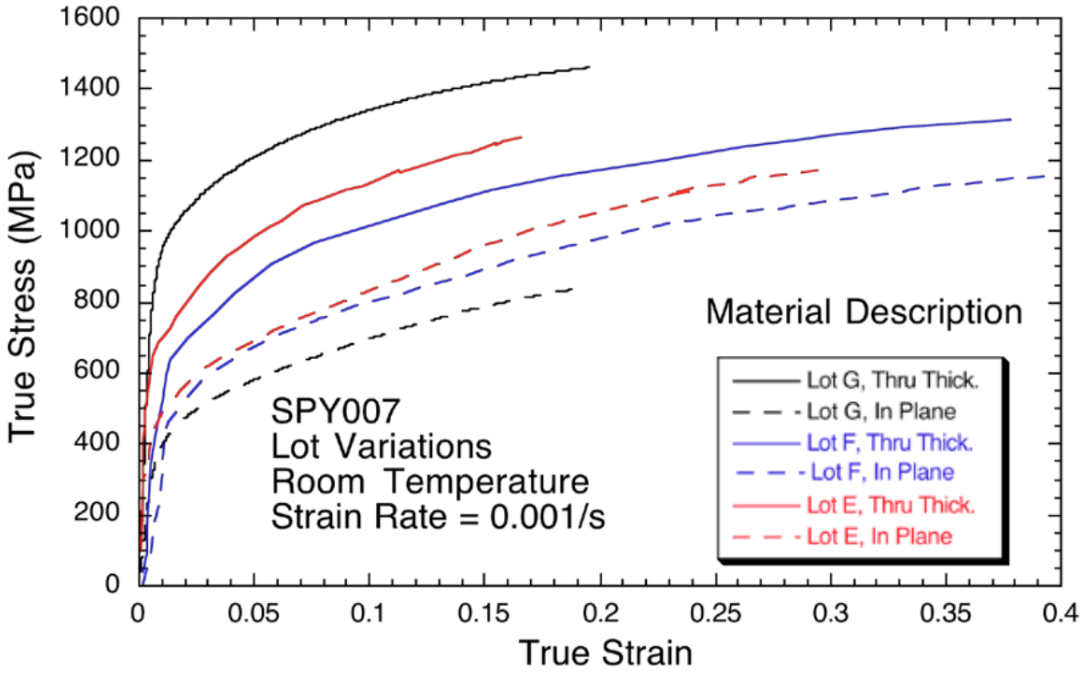

Figure 3: Example experimental data for Uranium provided by Shuh-Rong Chen [1]

To further complicate things, there are three choices available in FLAG for integrating the equivalent plastic strain ($\bar{\epsilon}^p$). The method is chosen by setting ps_inc ="flag","epic", or"conj". The default is ps_inc ="flag". There are subtle differences between the three choices. None of them are inherently wrong. However, it is very important that experimental data is analyzed with a particular choice of ps_inc in mind. Using the "epic" option the equivalent plastic strain rate is

$$\dot{\bar{\epsilon}}^p = \dot{\lambda}\sqrt{6\tau \cdot \tau}, \tag{21}$$

where $\dot{\lambda}$ is plastic rate multiplier of Equation 5. Using the "flag" option

$$\dot{\bar{\epsilon}}^p = \dot{\lambda}\sqrt{6det\left(\alpha_b\right)^{-2/5}\left(\tau \cdot \alpha^b\right) \cdot \left(\tau \cdot \alpha^b\right)}. \tag{22}$$

The "conj" option is derived by forcing the product of the effective stress and the equivalent plastic strain rate to be equal to the inner product of the stress and the plastic strain rate. This results in

$$\dot{\bar{\epsilon}}^p = \dot{\lambda}\sqrt{6\tau \cdot \alpha \cdot \tau}. \tag{23}$$

To determine $\dot{\lambda}$ from experimental data, look at Equation 5. This relates the plastic strain rate tensor to $\dot{\lambda}$ and the plastic flow tensor. The plastic flow tensor can be calculated for each of the six experiments stated above. The strain in the direction of loading for each experiment is used to calculate $\dot{\lambda}$, though the strains in other directions are non zero. The simple relationship is

$$\dot{\lambda} = \frac{\dot{\epsilon}_i^p}{\eta_i}, \tag{24}$$

the individual results of which are

$$\begin{aligned}
\dot{\lambda}_1 &= \tfrac{\dot{\epsilon}_1}{3\sigma_1(G+H)} \\
\dot{\lambda}_2 &= \tfrac{\dot{\epsilon}_2}{3\sigma_2(F+H)} \\
\dot{\lambda}_3 &= \tfrac{\dot{\epsilon}_3}{3\sigma_3(F+G)} \\
\dot{\lambda}_4 &= \tfrac{\dot{\epsilon}_4}{3\sigma_4 N} \\
\dot{\lambda}_5 &= \tfrac{\dot{\epsilon}_5}{3\sigma_5 M} \\
\dot{\lambda}_6 &= \tfrac{\dot{\epsilon}_6}{3\sigma_6 L}
\end{aligned} \quad . \tag{25}$$

The effective stress and equivalent plastic strain rates under uniaxial stress states are summarized in Table 1. The "Effective Stress" column is simply a summary of Equation 19. The "$\dot{\bar{\epsilon}}^p$ flag" column is found by combining Equation 22 with Equation 25, the "$\dot{\bar{\epsilon}}^p$ epic" column is found by combining Equation 21 with Equation 25, and the "$\dot{\bar{\epsilon}}^p$ conj" column is found by combining Equation 23 with Equation 25.

Table 1: Relationship between the equivalent plastic strain rate ($\dot{\bar{\epsilon}}^p$) and the plastic strain rate in the loading direction under uniaxial loading

Applied Stress	Effective Stress	$\dot{\bar{\epsilon}}^p$ flag	$\dot{\bar{\epsilon}}^p$ epic	$\dot{\bar{\epsilon}}^p$ conj
σ_{11}	$\lvert\sigma_{11}\rvert\sqrt{\frac{3}{2}(G+H)}$	$\frac{\dot{\epsilon}_{11}\sqrt{6\left[\left(\sqrt{2}H+\frac{\sqrt{2}}{2}G\right)^2+\frac{3}{2}G^2\right]}}{3\det(\alpha^b)^{1/5}(G+H)}$	$\frac{2\dot{\epsilon}_{11}}{3(G+H)}$	$\dot{\epsilon}_{11}\sqrt{\frac{2}{3(G+H)}}$
σ_{22}	$\lvert\sigma_{22}\rvert\sqrt{\frac{3}{2}(F+H)}$	$\frac{\dot{\epsilon}_{22}\sqrt{6\left[\left(\sqrt{2}H+\frac{\sqrt{2}}{2}F\right)^2+\frac{3}{2}F^2\right]}}{3\det(\alpha^b)^{1/5}(F+H)}$	$\frac{2\dot{\epsilon}_{22}}{3(F+H)}$	$\dot{\epsilon}_{22}\sqrt{\frac{2}{3(F+H)}}$
σ_{33}	$\lvert\sigma_{33}\rvert\sqrt{\frac{3}{2}(F+G)}$	$\frac{\dot{\epsilon}_{33}\sqrt{6\left[\frac{1}{2}(F-G)^2+\frac{3}{2}(F+G)^2\right]}}{3\det(\alpha^b)^{1/5}(F+G)}$	$\frac{2\dot{\epsilon}_{33}}{3(F+G)}$	$\dot{\epsilon}_{33}\sqrt{\frac{2}{3(F+G)}}$
σ_{12}	$\lvert\sigma_{12}\rvert\sqrt{3N}$	$\frac{\dot{\epsilon}_{12}}{\det(\alpha^b)^{1/5}}\sqrt{\frac{4}{3N}}$	$\frac{2\sqrt{3}\dot{\epsilon}_{12}}{3N}$	$\dot{\epsilon}_{12}\sqrt{\frac{4}{3N}}$
σ_{13}	$\lvert\sigma_{13}\rvert\sqrt{3M}$	$\frac{\dot{\epsilon}_{13}}{\det(\alpha^b)^{1/5}}\sqrt{\frac{4}{3M}}$	$\frac{2\sqrt{3}\dot{\epsilon}_{13}}{3M}$	$\dot{\epsilon}_{13}\sqrt{\frac{4}{3M}}$
σ_{23}	$\lvert\sigma_{23}\rvert\sqrt{3L}$	$\frac{\dot{\epsilon}_{23}}{\det(\alpha^b)^{1/5}}\sqrt{\frac{4}{3L}}$	$\frac{2\sqrt{3}\dot{\epsilon}_{23}}{3L}$	$\dot{\epsilon}_{23}\sqrt{\frac{4}{3L}}$

6 Example of an ideal fitting process

Here we present the fitting of the anisotropic plasticity model using a synthetic data set. We generated the synthetic data using Flag to run six simulations. The simulations included three uniaxial stress cases with the load applied normal to the symmetry planes and three pure shear cases with the shear applied in the symmetry planes. The material model used was a fictitious material including isotropic elasticity, a Hill plastic shape tensor, and a power law hardening flow stress (really Johnson Cook with the rate dependence parameter set to zero and the melt temperature left at 1e99 K to remove temperature dependence). The parameters used to generate the synthetic data are shown in Table 2.

Table 2: Parameters used to generate synthetic data

Bulk Modulus (MBar)	9.699
Shear Modulus (MBar)	3.45
Hill F parameter	1.0
Hill G parameter	1.0
Hill H parameter	1.375
Hill L parameter	5.164
Hill M parameter	4.573
Hill N parameter	3.581
Johnson Cook a (MBar)	0.01
Johnson Cook b (MBar)	0.05
Johnson Cook n	0.5

The synthetic data is shown in Figure 4. The data shows the linear regions prior to yielding. The linear regions associated with σ_{xx}, σ_{yy}, and σ_{zz} are all equal, and the slope is the elastic modulus (E). The linear regions associated with σ_{xy}, σ_{yz}, and σ_{xz} are also all equal, and the slope is the shear modulus (μ). Yield occurs at different stress levels in each of the loading directions, and the hardening is also different.

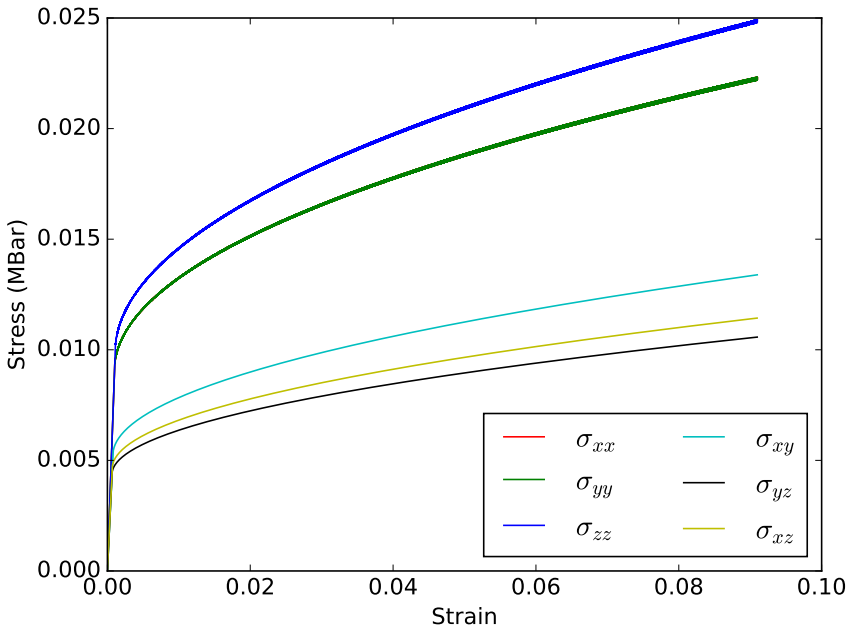

Figure 4: Synthetic stress vs. strain data.

The first step in fitting the data is to evaluate the slope in the linear region and calculate the plastic strain from the total strain For example

$$\begin{aligned} \epsilon^p_{xx} &= \epsilon_{xx} - \tfrac{\sigma_{xx}}{E} \\ \epsilon^p_{xy} &= \epsilon_{xy} - \tfrac{\sigma_{xy}}{2\mu} \end{aligned} \quad . \tag{26}$$

The stress is plotted against plastic strain in Figure 5. Comparing Figures 5 and Figure 4, you can conclude that, except right at the onset of plastic deformation, the elastic strain is negligible, and this step is unnecessary. The step is trivial to perform with this synthetic data, but if there are not clear linear regions in real experimental data it would be acceptable to treat total strain as plastic strain.

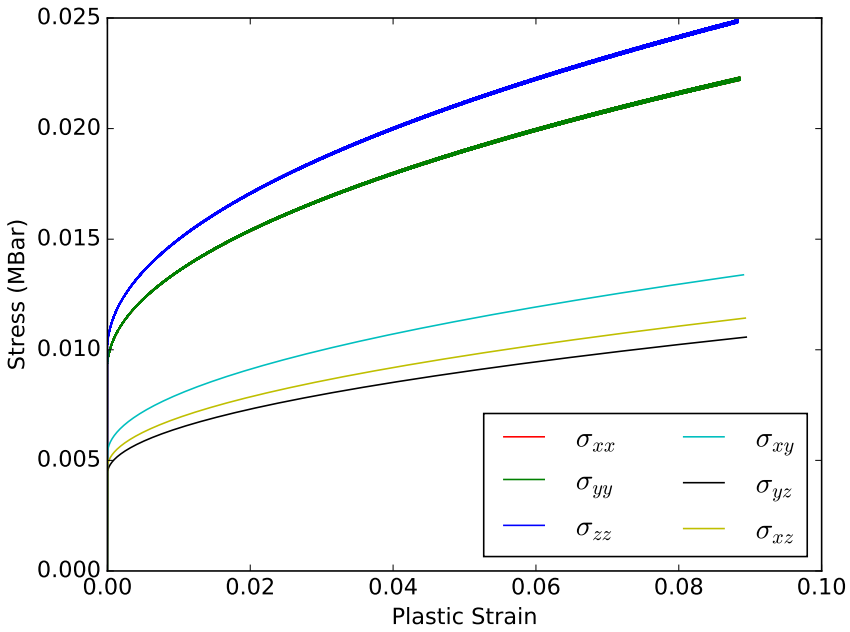

Figure 5: Stress vs. plastic strain.

Finding the Hill surface parameters is easy when the elastic regions are clear. The yield stresses are determined by some threshold departure of the experimental data from the straight line in stress-strain space or a plastic strain that exceeds some threshold. Then Equations 20 are applied to determine the parameters. Once we find those parameters we apply the effective stress equations in Table 1 and plot the effective stress against the plastic strain. These are shown in Figure 6. The curves are still different from each other. This is because with the Hill model, the equivalent plastic strain ($\dot{\epsilon}^p$) is not equal to the plastic strain in the loading direction.

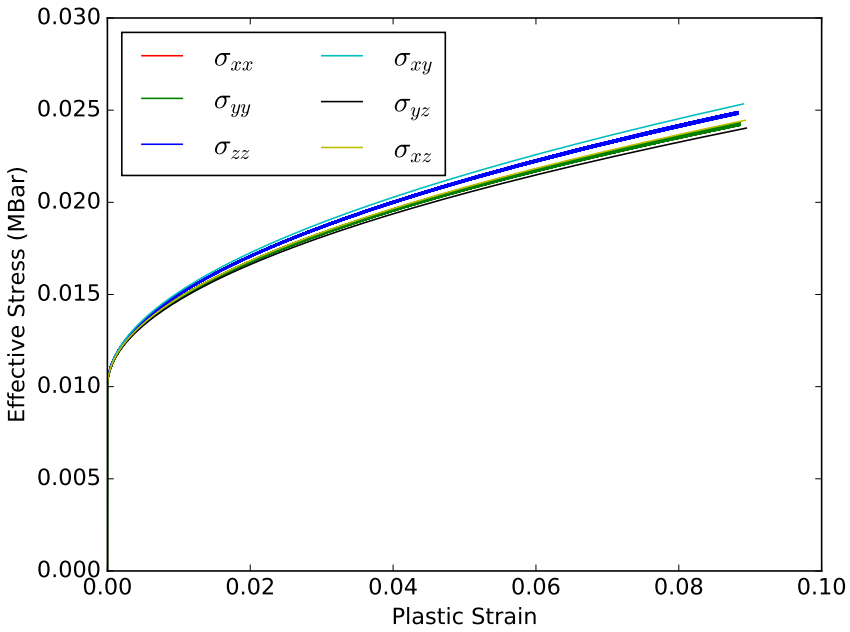

Figure 6: Effective stress vs. plastic strain.

Equations for determining the equivalent plastic strain given the strain in the loading direction and the Hill parameters are shown in Table 1. There are three choices for $\dot{\bar{\epsilon}}^p$ depending on the setting of *ps_inc* in Flag. After applying the *conj* version of the corrections we plot effective stress against equivalent plastic strain in Figure 7. Now, all the curves are on top of each other. This single curve is the curve that should be used to fit the flow stress model.

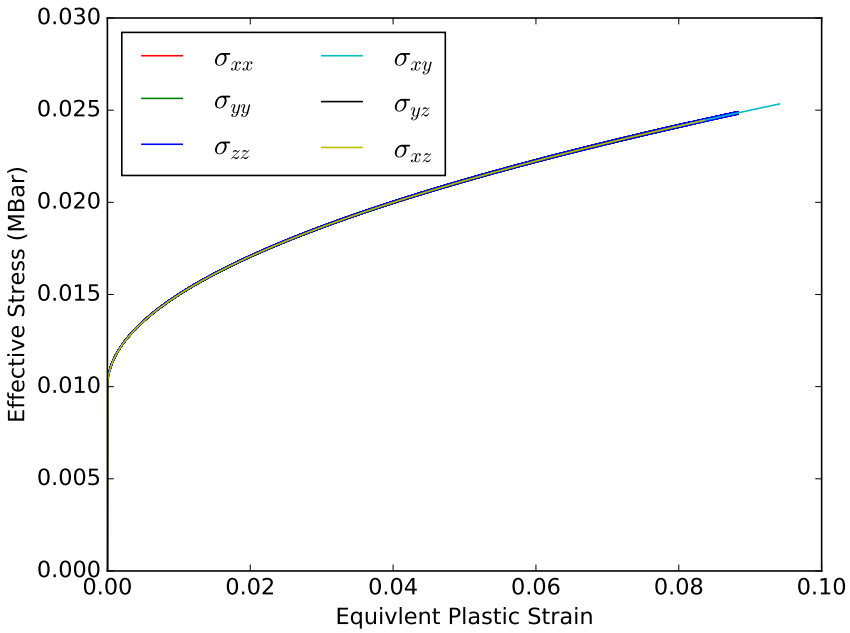

Figure 7: Effective stress vs. equivalent plastic strain.

An alternative strategy that might be employed if the data is noisier than this synthetic data or the yield stresses are more difficult to determine would be to simply optimize the Hill parameters F-N, by minimizing the difference between all the curves in $\bar{\sigma} - \bar{\epsilon}^p$ space. That process was carried out using the original synthetic data, but this time fitting for *ps_inc=flag*. Results of that fit are shown in Figure 8. The *ps_inc=flag* fit is plotted using + symbols and the *ps_inc=conj* fit is shown as a solid line. It is obvious that there will be a significant difference between the appropriate flow stress model parameters for the two choices of *ps_inc*. The process also resulted in different Hill parameters. The elasticity parameters remained the same. The Hill and hardening parameters are listed in Table 3.

Table 3: Parameters found by fitting the synthetic data using *ps_inc=flag*

Hill F parameter	0.96
Hill G parameter	0.96
Hill H parameter	1.43
Hill L parameter	5.758
Hill M parameter	4.962
Hill N parameter	3.581
Johnson Cook a (MBar)	0.01
Johnson Cook b (MBar)	0.0593
Johnson Cook n	0.52

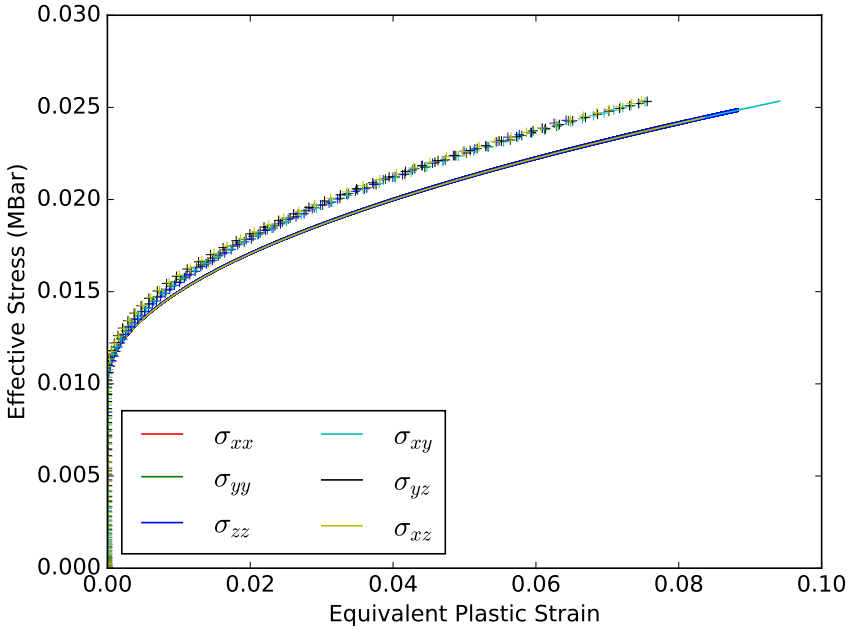

Figure 8: Effective stress vs. equivalent plastic strain.

We performed the simulations in flag again but using the *ps_inc=flag* parameters, and the results are

plotted in Figure 9. The original synthetic data is plotted using a solid line and the results using the new fit are plotted using + symbols. The + symbols fall on top of the original data demonstrating that with significantly different parameters the two models give largely equivalent results. The point is that any of the three choices for *ps_inc* are valid, but the data must be fit with that choice in mind.

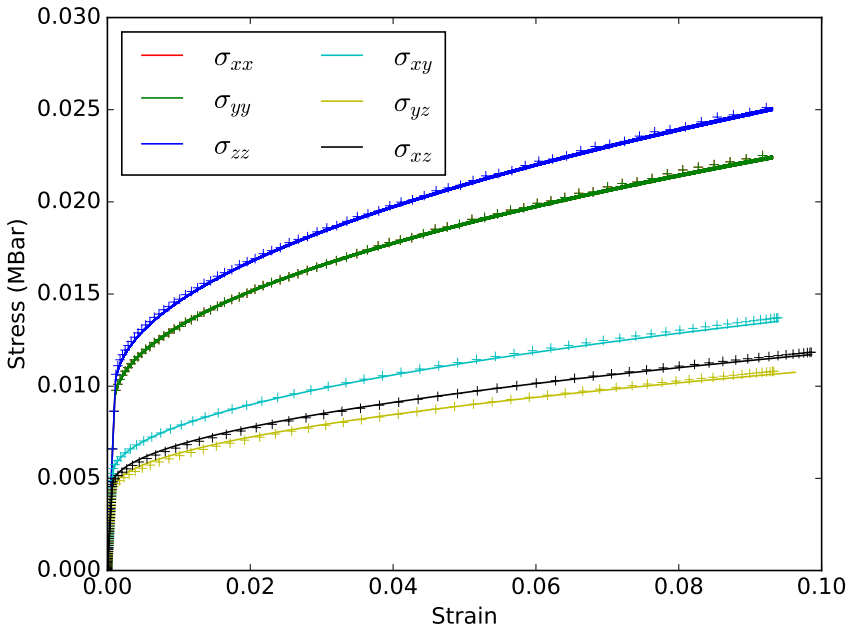

Figure 9: Comparison of synthetic data to simulations using the *ps_inc=flag* fit to the synthetic data.

7 Conclusions

Here we have described the theory behind the anisotropic elasto-plasticity model implemented in FLAG. Stress updates are carried out in a frame attached to the material which allows for constant anisotropic properties ($\boldsymbol{C}$ and $\boldsymbol{\alpha}$). Improved computational efficiency is achieved by transforming the equations to the B-basis. We describe the process of fitting the anisotropic shape tensor $\boldsymbol{\alpha}$ as well as a flow stress model. Finally, we provide an example of fitting $\boldsymbol{\alpha}$ and a simple power law flow stress model. This example demonstrates the importance of matching the plastic strain increment model (*ps_inc*) to the flow stress fit

parameters.

References

[1] George T. Gray III. et.al., *Characterization of depleted-uranium strength and damage behavior*, Tech. Report LA-UR-12-26963, MRT#4521, Los Alamos National Laboratory, 2012.

[2] R. Hill, *A theory of the yielding and plastic flow of anisotropic metals*, Proceedings of the Royal Society of London A: Mathematical, Physical and Engineering Sciences **193** (1948), no. 1033, 281–297.

[3] J.W. House S.R. Chen P.J. Maudlin, J.F. Bingert, *On the modeling of the taylor cylinder impact test for orthotropic textured materials: experiments and simulations*, International Journal of Plasticity (1998).